How to cite: *Angew. Chem. Int. Ed.* **2022,** *61,* e202208647
International Edition: doi.org/10.1002/anie.202208647
German Edition: doi.org/10.1002/ange.202208647

Self-assembly

Cyanine Dye Coupling Mediates Self-assembly of a pH Sensitive Peptide into Novel 3D Architectures

Rita Fernandes, Suvrat Chowdhary, Natalia Mikula, Noureldin Saleh, Katerina Kanevche, Hans v. Berlepsch, Naoki Hosogi, Joachim Heberle, Marcus Weber, Christoph Böttcher, and Beate Koksch**

Abstract: Synthetic multichromophore systems are of great importance in artificial light harvesting devices, organic optoelectronics, tumor imaging and therapy. Here, we introduce a promising strategy for the construction of self-assembled peptide templated dye stacks based on coupling of a de novo designed pH sensitive peptide with a cyanine dye Cy5 at its N-terminus. Microscopic techniques, in particular cryogenic TEM (cryo-TEM) and cryo-electron tomography technique (cryo-ET), reveal two types of highly ordered three-dimensional assembly structures on the micrometer scale. Unbranched compact layered rods are observed at pH 7.4 and two-dimensional membrane-like assemblies at pH 3.4, both species displaying spectral features of H-aggregates. Molecular dynamics simulations reveal that the coupling of Cy5 moieties promotes the formation of both ultrastructures, whereas the protonation states of acidic and basic amino acid side chains dictates their ultimate three-dimensional organization.

Introduction

The formation of supramolecular structures is an essential prerequisite in natural systems for physiological and/or structural function. Natural photosynthetic systems use proteins as scaffolds for chromophores to facilitate a coherent energy transfer for moving excitation energy. The resulting delocalized excitons are spread in a wavelike manner over the interacting dyes.[1] Just because of this feature, molecular excitons have gained considerable interest arising from their potential applications in artificial light harvesting, organic optoelectronics,[2] nanoscale computing,[3] and tumor imaging and therapy.[4] The realization of devices using excitonic systems requires controlled delocalization of excitons along specific structures. Currently, deoxyribonucleic acid (DNA)-based nanotechnology has emerged as an effective and accessible method in the design of scaffolded chromophore aggregate systems at subnanometer scales according to simple design rules.[5] Cyanines with different lengths of the polymethine chain (PIC, Cy3, Cy5) have been demonstrated to form strongly coupled aggregates templated on the DNA strands similar to J- or H-aggregates in terms of their molecular packing, spectroscopy, and energy transfer properties.[6] However, the accuracy and the depth of the available structural data in DNA nanotechnology have remained limited[7] compared to the structural data that are routinely generated in the field of protein design.[8] Therefore, spectroscopic methods supported by molecular modelling have been the work horses in studies involving DNA.

In contrast to the remarkable progress achieved in recent years in understanding the DNA-templated systems, there have been very few systematic studies of peptides as scaffolds.[4a,9] This is surprising since synthetic peptides offer several advantages, namely precise control over amino acid composition, chain length and numerous chemical functionalities of amino acid side chains,[10] as well as straightforward synthesis procedures.[11] In addition, peptides can be designed to self-assemble in aqueous solvents, adopt a wide variety of morphologies, such as fibers, tubes, vesicles, and membranous or fibrillar networks and last but not least can

[*] R. Fernandes, S. Chowdhary, Prof. Dr. B. Koksch
Department of Chemistry and Biochemistry,
Freie Universität Berlin
Arnimallee 20, 14195 Berlin (Germany)
E-mail: beate.koksch@fu-berlin.de

N. Mikula, Dr. N. Saleh, Dr. M. Weber
Mathematics for Life and Materials Sciences,
Zuse Institute Berlin
Takustraße 7, 14195 Berlin (Germany)

K. Kanevche, Prof. Dr. J. Heberle
Department of Physics, Experimental Molecular Biophysics,
Freie Universität Berlin
Arnimallee 14, 14195 Berlin (Germany)

Dr. H. v. Berlepsch, Dr. C. Böttcher
Research Center for Electron Microscopy and Core Facility
BioSupraMol, Freie Universität Berlin
Fabeckstraße 36a, 14195 Berlin (Germany)
E-mail: christoph.boettcher@fzem.fu-berlin.de

N. Hosogi
Nakagami JEOL, Ltd
Akishima Tokyo 196 (Japan)

be structurally well characterized by cryo-TEM at high resolution.[8d–e]

A key aspect for the applicability of peptide-based materials is the possibility to precisely control and tune the formation of well-defined morphologies. This can be achieved by rational design using known sequence-structure relationships and/or by changing environmental cues such as temperature and pH.[12] There are several examples of stimuli-responsive supramolecular assemblies based on β-sheet adopting peptides and, to a lesser extent, on α-helix forming peptides.[13] In the latter case, examples of the controlled assembly of fibers,[14] nanotubes,[15] and hydrogels[16] by changes in pH and temperature have been reported. Whereas important advancements toward structural elucidation at the atomic level have been made,[8d] the design of primary sequences capable of inducing desired molecular interactions that lead to highly organized assembly processes and structures still remains challenging.

Here we present a simple, chemically accessible pH-sensitive peptide combined with an *N*-terminal coupled Cy5 as chromophore. We studied its self-assembly behavior by a combination of spectroscopic and microscopic, notably cryogenic TEM (cryo-TEM), and cryo-electron tomography technique (cryo-ET), as well as molecular dynamics simulations. We were in particular interested in how the tuneable peptide scaffold affects the packing characteristics of chromophores and hence their optical features and, vice versa, how the dye modifies the peptide packing architecture. Compared to the neat peptide system a restructuring of the peptide scaffold was expected upon covalent coupling of an organic dye molecule, alone for steric and hydrophobic reason. Moreover, in multichromophore systems the electronic interaction between chromophores acts as an additional driving force for self-aggregation. It is well documented for numerous dye molecules, in particular cyanines,[17,18] that they are able to form mesoscopic structures spontaneously from monomers in aqueous medium. Therefore, a mutual influence of the self-aggregation of the peptides, on the one hand, and of the dye molecules, on the other hand, is expected.[19] An additional factor considered for this study was the capability of the designed peptide (**STAP1**) of responding to pH changes by forming different supramolecular structures. The detailed analysis revealed two different but highly ordered ultrastructures on the micrometer scale depending on pH, both spectroscopically characterized by face-to-face stacking motifs of the Cy5 moieties namely H-dimers and higher H-aggregates, respectively.

To our knowledge, the dye-peptide conjugate (**STAP1**) described herein represents the first of its kind being able of assembling into two distinct highly ordered structures based on complementary effects of excitonic dye coupling and pH triggered peptide interactions. Our current work focuses on the detailed spectroscopic and structural characterization of the obtained supramolecular assemblies.

Results and Discussion

Peptide Design, Self-Assembly and Optical Characterization

The peptide investigated here is based on sequences previously published by our group,[20] and it follows the design rules for the formation of α-helical coiled-coil bundles.[21,22] This folding motif is characterized by the repetition of seven amino acids referred to as the heptad repeat, denoted $abcdefg_n$, where positions *a* and *d* are hydrophobic, positions *e* and *g* are occupied by charged amino acids, and the remaining positions *b*, *c* and *f* are generally polar residues.[23] As illustrated in Figure 1, the stimuli-triggered aggregating peptide (**STAP1**) described here consists of a regular distribution of amino acids in a *hpphppp* pattern. Leucine residues drive self-assembly due to hydrophobic effects and serine residues increase peptide solubility. Eight lysines and eight glutamates were incorporated to form inter- and intrahelical salt bridges. Since **STAP1** has 16 ionizable side chain residues, it is highly responsive to changes in pH. At the N-terminus, we coupled a cationic pentamethine cyanine (Cy5). Cyanines are excellent model dyes because of their well-documented ability to form multichromophore assemblies by self-aggregation in solution due to dispersive forces (π-π interaction). In addition, the large extinction coefficient facilitates spectroscopic detection.[19,24–26]

As a control peptide, **STAP2** was synthesized with a free N-terminus, i.e. lacking the dye. (HPLC data of both peptides are given in Figures S1 and S2). Circular dichroism (CD) spectroscopy was applied to probe for peptide conformation and stability in solution. CD analysis revealed the typical helical motif with the double minima around 208 and 222 nm for all pH conditions (Figure S3a) and almost

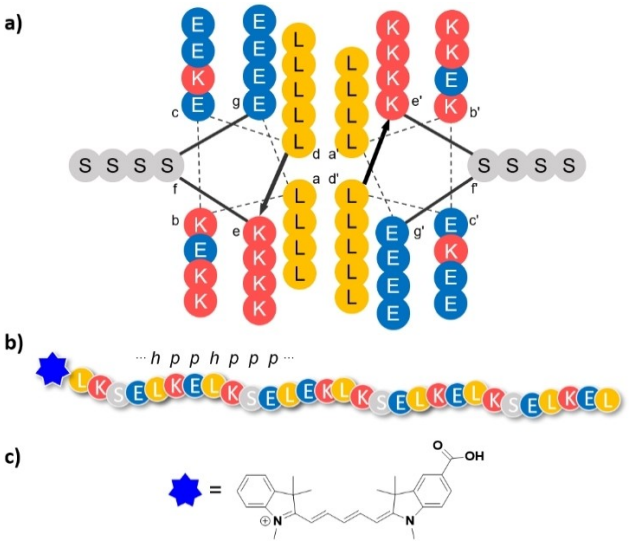

Figure 1. a) Helical wheel representation of the primary sequence of **STAP1** and **STAP2**. b) Linear representation of **STAP1** showing the *N*-terminal Cy5 dye indicated by a blue star; **STAP2** contains no dye. c) Cy5 structure: glutamic acid (blue circles), leucine (yellow circles), lysine (red circles) and serine (grey circles), Cy5 (blue star).

independent of thermal history (denaturation) (Figures S3b–d). **STAP2** is assumed to be in a single α-helical conformation. Under acidic conditions, **STAP2** self-assembled into long and flexible fibers made by the lateral association of thin fibrils, whereas under neutral conditions only ill-formed nano-aggregates were observed (Figure S4).

The situation changes significantly for the dye-conjugated peptide **STAP1**. Its CD spectra at pH 3.4 and 7.4 show again the double minima characteristic of an α-helical conformation (Figures S5A and S5B), but in particular at neutral pH the minimum at 222 nm is enhanced with respect to **STAP2**. The thermal stability of **STAP1** was investigated by recording the ellipticity as a function of temperature (Figures S5C–F). At pH 7.4 an initial denaturation experiment resulted in a melting temperature (T_M) of ≈47 °C. Upon returning to room temperature the samples revealed a significant increase in the ellipticity and in a subsequent denaturation experiment T_M increased to ≈73 °C (Figure S5D). Similar annealing effects have been previously described for the formation of highly ordered α-helical fibers.[27] It is also noteworthy that the ratio of signal intensity at 222 nm relative to that at 208 nm increased after denaturation. Similarly distorted spectra have been occasionally observed and attributed to scattering effects due to the formation of large aggregates in solution.[28] In contrast, at pH 3.4, **STAP1** shows no defined thermal transition, i.e., the peptide is highly stable up to 95 °C (Figure S5C).

Depending on the spatial arrangement of dye molecules within the aggregate (Figure S6 shows a schematic view), different optical spectra can be observed. Thus, the spectroscopic characteristics of the dye allow for further probing of the aggregates' structures by means of steady-state absorption and fluorescence spectroscopy as well as linear dichroism (LD) spectroscopy. First, free Cy5 dye was characterized by absorption spectroscopy (Figure S7). In MeOH the typical spectrum of cyanine monomers with a main absorption band at approximately 640 nm (labelled in Figures 2 and S7 as "M") and two shorter-wavelength vibrational sub-

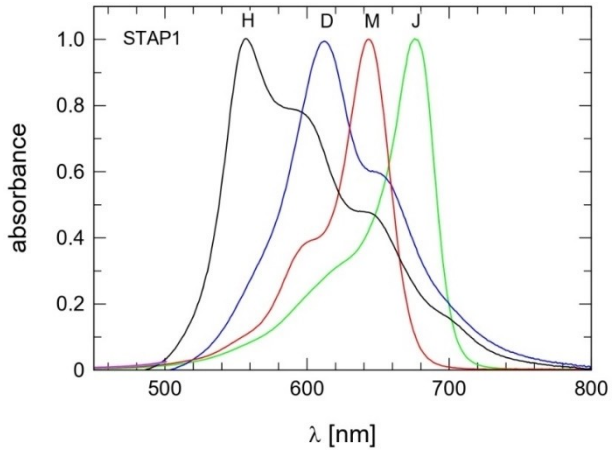

Figure 2. Normalized absorption spectra of **STAP1** solutions at different pH values: 3.4 (black line), 7.4 (blue line), 11 (green line). **STAP1** concentration: ≈0.5 g L^{-1}. Overlaid for comparison is the absorption spectrum of free Cy5 in MeOH (red line).

bands was observed. In contrast, in buffered aqueous solutions at different pH values a new blue-shifted absorption band of the free dye at around 590 nm (labelled in Figure S7 as "D") evolved, which we ascribe to H-dimers. The high propensity of free Cy5 to form aggregates is most clearly observed at pH 3.4 (black trace in Figure S7). These spectroscopic studies were extended to Cy5 in the context of the **STAP1** peptide in buffers of different pH values. The spectra obtained (Figure 2) indicate the appearance of different classes of aggregates, for which the absorption bands are labelled "H" for H-aggregates, largely observed at pH 3.4, "D" for H-dimers of the type mentioned above, the major species at pH 7.4, and "J" for J-aggregates, mainly present at pH 11.[6a] The three prototypical spectra most likely represent mixed populations and contain contributions from residual monomers, that is, non-aggregated peptide. Moreover, the large width of the absorption band together with the appearance of a shoulder at around 700 nm for the H-aggregates might indicate an additional (Davydov) splitting of the absorption spectrum due to an oblique geometric configuration of the involved Cy5 chromophores.[29] The spectral features are very close to those of reported DNA-templated tetramer aggregates ("DNA Holliday junction scaffolds" (HJ)).[5e,6e] We also investigated in detail the fluorescence behavior of the solutions. Figure S8 for example shows the results for pH 7.4. The emission spectrum is mirror-symmetric to the absorption spectrum and almost identical with the emission spectrum of the free dye Cy5 (not shown). This finding is a strong indication that this emission is due to residual monomers, while the H-dimers (D) are obviously non-fluorescent as generally expected for face-to-face stacked H-aggregates.[29] A quite similar fluorescence behavior was observed also for the H-aggregates (pH 3.4)[5e,6e] and for pH 11.

Altogether these findings provide evidence that residual monomers (non-aggregated peptide) are ultimately responsible for the fluorescence emission. The absence of a resonant emission for the J-type aggregates formed at pH 11 is surprising, because these normally show strong fluorescence. Information about the molecular packing orientation of Cy5 moieties within the assemblies was provided by polarized absorption spectra recorded on samples oriented by the streaming field in a Couette flow cell. Detected is the linear dichroism (LD) spectrum, which is the difference in absorption of light parallel and perpendicular to the orientation direction. A positive LD signal indicates an orientation of the responsible transition dipole moment of dye molecules parallel to the flow, i.e. parallel to the long axis of corresponding aggregates, while a negative signal points to an orientation perpendicular to the flow. Exemplary spectra are presented in Figures S9 and S10.

Morphology of Aggregates

For an initial structural characterization of **STAP1** buffered at pH values of 3.4, 7.4 and 11 we used negative-staining

transmission electron microscopy (TEM). The images reveal the formation of highly ordered micrometer scale aggregates at pH 3.4 and 7.4. While the aggregates at pH 3.4 were spontaneously formed after buffer addition, defined aggregates at pH 7.4 were observed only after thermal treatment. The samples had to be heated to 95 °C with subsequent slow cooling (at a rate of $\approx 3\,^{\circ}C\,min^{-1}$) to ambient temperature. Otherwise the solutions showed only ill-defined assemblies (Table 1 and Figure S11). At pH 11, small disordered assemblies, probably helical oligomers, were observed under all conditions. The absence of any ordered mesoscopic structure is the reason why we did not explore this case more thoroughly and restricted ourselves to neutral and acidic solvent conditions. Experiments with the control peptide **STAP2** showed formation of long, thin fibrils at pH 3.4, whereas small micelle-like objects were found at pH 7.4 (Figure S4).

Detailed structural characterization was performed by means of AFM imaging and cryogenic TEM (cryo-TEM) techniques, in particular cryo-electron tomography (cryo-ET). Notably, the morphologies of mesoscopic aggregates turned out to be highly ordered but completely different in their ultrastructural organization, as described below.

Assembly Structure at pH 7.4

At pH 7.4, three-dimensional rod-like aggregates with widths in the 90–300 nm range and lengths up to several micrometers are observed (Figures 3a,c). At higher magnification, layered striations perpendicular to the long axis of aggregates at a repetitive distance of 4.4 nm are prominent (Figures 3b, S12 and S13).

If the rods 3D reconstructed from cryo-ET data are rotated about the long axis, additional striations parallel to the rod axis with exactly the same repetitive distance (4.4 nm) are observed (Figure 3d) and only once again by subsequent 180° rotation. If the motif of Figure 3d is tilted by 90° forward-facing (Figure 3e) the rods reveal parallel strands again at a repetitive spacing of 4.4 nm, so that the overall rod structure can be described by a stacked arrangement of strands arranged in a tetragonal manner as illustrated in the scheme of Figure 3h. The 4.4 nm spacing distance here observed is in line with previously reported values for striated fiber-forming coiled-coils[8d,30] but the surprising new observation is, that the filaments here are not oriented parallel to the rod long-axis, as was usually observed, but in perpendicular direction. It must be noted that a peptide arrangement similar to the one proposed for the gigadalton coiled-coil fibers of Sharp et al.[8d] in which the peptide strands are hexagonally packed within the fibers, was initially also expected for the **STAP1** system. However, this arrangement was ultimately rejected for **STAP1** as it was not found to be consistent with the cryo-ET data obtained here.

We applied near-field spectroscopy (nano-FTIR) to obtain information on the **STAP1** folding motif within these aggregates (Figure S14). All recorded spectra are dominated by two bands at 1659 cm^{-1} and 1551 cm^{-1}; these correspond to the C=O stretching vibration (Amide I) and the combined N–H bending and C–N stretching vibrations (Amide II), respectively. The band position of the Amide I at 1659 cm^{-1} indicates an α-helical folding motif.[31] Besides enabling assigning secondary structure, nano-FTIR spectroscopy is also sensitive to the orientation of particular molecular vibrations. As previously shown,[31] highly oriented protein layers show strong Amide I and negligible Amide II absorption. The comparable intensity of both protein bands in our case indicates that the α-helices are not homogeneously oriented, i.e., not all helices are oriented perpendicularly to the surface.

Assembly Structures at pH 3.4

The aggregates at pH 3.4 adopt a morphology completely distinct from that of rods observed at neutral pH, in both shape and size. Although the ultrastructure is also remarkably well-defined, these structures are primarily two-dimensional and thus membrane-like layers (Figure 4a). Due to the large size these peptide membranes are also observed to be folded or crinkled. At the edges, where a folded membrane is orientated perpendicular to the image plane, the profile of the membrane becomes visible revealing a thickness of about 9 nm and a regular internal structural organization (Figures 4b,c).

In several cases, the stacking of more than one membrane layer is observed by cryo-ET due to a multilayered rolled-up type structure and accounts for the thickness values up to 71 nm observed using AFM (Figure 4e). The flat membrane layer itself comprises a hexagonal pattern of very high regularity and (Figure 4a) even if multilayered the membranes show only this particular motif in projection due to a perfect stack alignment. Its detailed volume structure is discussed in the next section. By means of nano-FTIR, two bands (Amide I and Amide II) at 1655 cm^{-1} and 1551 cm^{-1} are also observed, indicating that **STAP1** adopts an α-helical folding motif also within this morphological type (Figure S14). A third prominent vibrational band at 1732 cm^{-1} is apparent for some objects under this acidic regime. This could be attributed to either the

Table 1: Effect of pH on **STAP1** aggregation.

pH	Morphology	Spectral Type	Preparation
3.4	membranes	H-aggregate	formed spontaneously
7.4	striated rods	H-dimer	formed after thermal treatment
11	amorphous	J-aggregate	independent of preparation

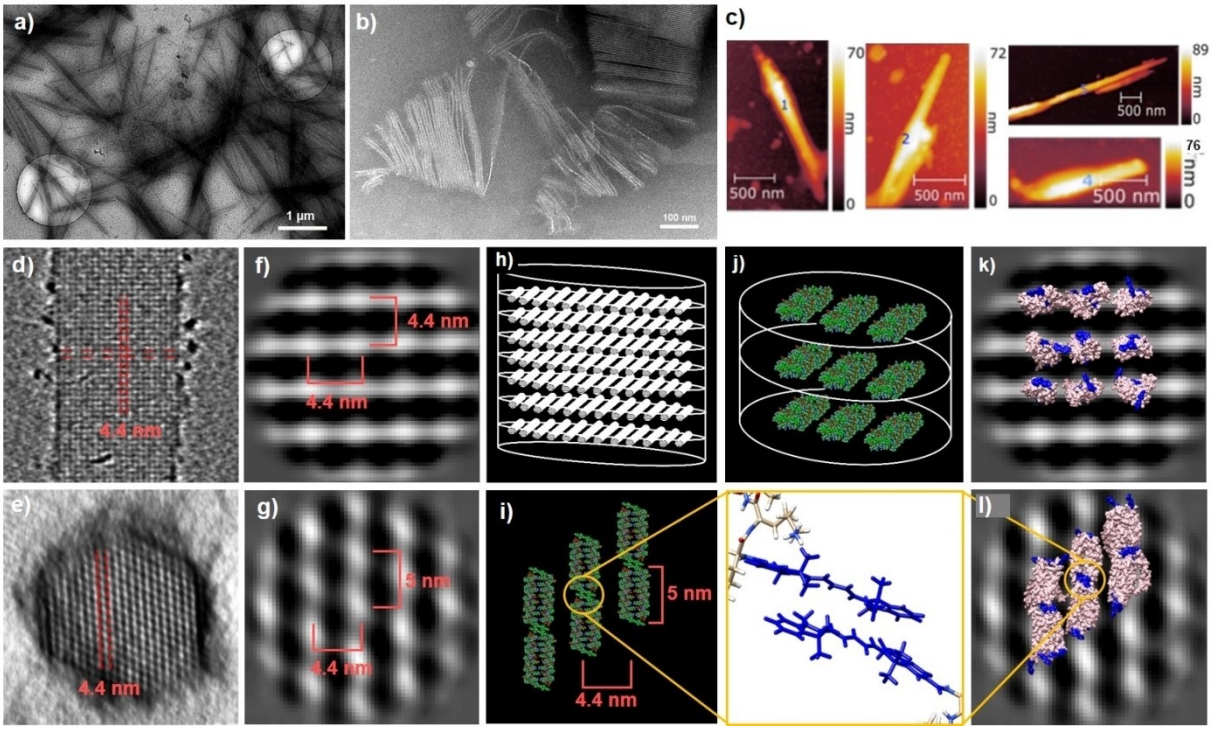

Figure 3. Structural morphology of **STAP1** at pH 7.4: a) Cryo-TEM overview showing a dense population of **STAP1** rod assemblies. b) Negative staining (1 % PTA at pH 7.4) TEM of **STAP1** highlighting the layered supramolecular organisation and also indicating partial disintegration into individual layers. c) Topographical AFM height images (integers indicate sample numbers) of **STAP1** rod assemblies. d, e) Volume reconstruction of a rod (detail) based on cryo-ET data: d) Side view and e) top view of d) at 90° forward facing. The red traces represent the repetitive 4.4 nm spacing between striations. f) Sum image (detail) of a rod side view (note inverted contrast) obtained by averaging 5000 slice motifs along the reconstructed rod volume where high density motifs at 4.4 nm distance indicate the orthogonal strand orientation. g) Sum image of rod top view layers from (e) (perpendicular to f) obtained by averaging 5000 individual layers motifs along the reconstructed rod volume. In each linear strand repetitive motifs of lower density at a 5 nm repeat distance (marked with the red semi-bracket) is evidenced. Adjacent strands are 4.4 nm apart at which 5 nm low density motifs are shifted by 2.2 nm against each other. h) Schematic illustration of the spatial strand arrangement in a rod. i) Proposed arrangement of **STAP1** at pH 7.4 within a layer in agreement with experimental dimensions, electron density pattern (cf. (f), (g)) and LD spectra. j) Starting geometry of **STAP1** used for MD simulations consisting of three molecular layers as shown in i) in a spatial arrangement in full agreement with dimensions and density data obtained by electron microscopy. k) and l) Fit of **STAP1** after 10 ns MD simulations into the density map of (f) and (g), respectively, using the start geometry shown in (j). The top view of the arrangement of **STAP1** at pH 7.4 still fit the repetitive low density areas along the striations of (g) to the location of Cy5 stacks (blue regions). The inset shows the stacked arrangement of the Cy5 moiety in accordance with LD spectra. Conditions: 0.1 mM of **STAP1** in 50 mM phosphate buffer, pH 7.4 and after a heating/cooling cycle (95 to 20 °C at 3 °C min^{-1}).

C=O stretch from the citrate buffer or the protonation of glutamic acid, with its pK_a value of around 4.[32]

We used additional image processing procedures (for details see Supporting Information) for both types of assemblies to gain more precise structural information from the cryo-ET data for the fitting of consistent molecular models.

Processing and Modelling of pH 7.4 Rod Structures

For the rod assemblies at pH 7.4, an averaging over manifold side-view layers taken from the reconstructed 3D volume was performed to obtain sum images of improved signal-to-noise ratio (Figure 3f). Individual stack layers are remarkably well resolved and oval repetitive density spots along the stacks mark the position of individual forward-facing strands. The same approach was applied for the motif perpendicular to the stacked planes (top view) and results in the sum image of Figure 3g. Both sum images provide more details than does the raw tomography data (Figures 3d, e), e.g. even small repetitive density variations in the structure can be revealed and validate a structure resolution level of at least 10 Å obtained under the chosen microscopic and data processing conditions (see details in the Supporting Information). In the top view orientation (Figure 3g), the linear strands, which are the elementary building blocks of the rod morphology, reveal repetitive motifs of low (grey) and high (white) electron density along the strands at a 5 nm repeat distance. As mentioned above, if oriented perpendicular to the top view (Figure 3f), the forward-facing strands appear oval with dimensions of ≈3 nm × 1.5 nm. Upon accepting that two molecular strands in a side-by-side arrangement would reasonably fit the cross section, we suspect an antiparallel arrangement of the peptide strands, stabilized by π-π stacking of pairs of Cy5 dye molecules

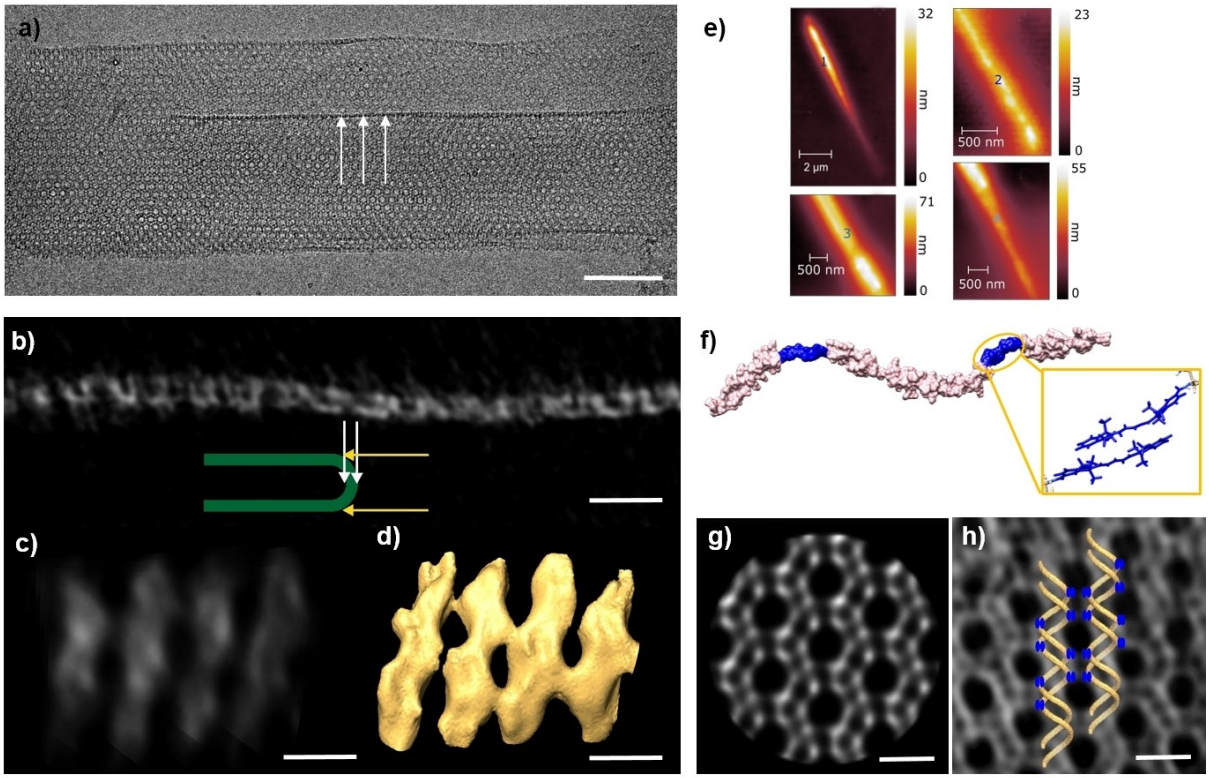

Figure 4. Structural morphology of **STAP1** at pH 3.4. a) Cryo-TEM of **STAP1** highlighting a layered supramolecular organization with arrows pointing to the membrane layer orientated parallel to the incident electron beam and revealing the membranes density profile. Bar is 50 nm. b) Top view and c) side view orientation of the membrane (indicated by the scheme showing the geometrical orientation of the membrane and projection direction highlighted by white and yellow arrows, respectively). The cryo-tomographic volume data are shown in Voltex representation using AMIRA software (Thermo Fisher Scientific) with inverted contrast. Bar is 25 nm. d) Surface representation of c) revealing the left-handedness of double super-helices. e) Topographical AFM height images (integers indicate sample number) give thickness values up to 71 nm indicating multi-layered roll-up of membranes. f) Proposed arrangement of **STAP1** strands at pH 3.4 taken after 10 ns MD simulations where stacking between two Cy5 moieties (blue regions) leads to the longitudinal elongation and twisting towards a helical ultrastructure. Note the C-terminal connection of the central peptide strands. g) Average of the hexagonal pattern of 60 motifs taken from areas of (a) where the membrane is orientated perpendicular to the incident beam. h) Fit of two modelled double super-helical strands in the volume of the 3D reconstructed pattern (g) is the top view thereof, which illustrates the formation of the underlying hexagonal motif. For original 3D super-helix data see Figure S15. The repetitive orientation of the Cy5 pairs (blue) allows for their additional lateral stacking and eventually leads to the formation of assemblies with a two-dimensional geometry. Conditions: 0.1 mM of **STAP1** in 50 mM citrate buffer, pH 3.4.

(Figure 3i). This model would fit the dimensions and also explain the regular low-density areas along the strands due to the tilted orientation of the dye stack. A conceivable parallel arrangement would create chemically different environments at the end-caps, namely the dye stack at one end, and two O-termini of leucines at the other. The consequence would be an immediate further terminal stacking interaction of the dye (formation of tetramers, along or perpendicular to the strands long-axis), in other words the formation of molecular bilayers as e.g. found for individual strands at pH 3.4 (Figure 4f). This would eventually lead to 10 (2×5) nm long sections of high density in the according density map along the strands, what we did not observe. Also tetramers were not found by spectroscopy as was e.g. the case with membranes at pH 3.4. Moreover, the dominance of dimers (D) in the absorption spectrum of these aggregates and the corresponding negative LD signal (Figure S9), which points to an orientation of the responsible transition dipole moment of Cy5 molecules perpendicular to the long axis of aggregates support the proposed molecular arrangement of Figure 3i. The distance between (antiparallel) strands and layers is 4.4 nm and 5 nm between the dye stacks along the antiparallel peptide arrangement.

Molecular dynamics (MD) simulations were performed by extending the antiparallel starting geometry of Figure 3h for **STAP1** at pH 7.4: twelve peptide strands were arranged in a plane and three such layers were stacked (Figures 3j and S16a). After a simulation time of 10 ns only small changes were observed, indicating that the suggested structure represents a stable geometry at pH 7.4 (Figure S16b). Notably, **STAP1** does not tend to adopt a coiled-coil conformation but rather single peptide chains remain parallel arranged within each layer (Figure 3k). This is obviously a consequence of π-π stacking of the Cy5 moieties of two neighboring peptide strands in antiparallel orientation, preventing their free rotation around the long-axis towards an expected coiled-coil formation. This two strand structure is additionally stabilized by salt bridges between

lysine and glutamate, which in this case are pointing towards the core (Figure S16c). The designed heptad repeats allow for the additional presentation of a hydrophobic edge of leucine that further stabilizes a side-by-side arrangement of the so formed "double strands" within the layers and prevents the disintegration into individual strands. The exact locating of the strands rotational position (Figure 3k) due to the combined molecular interactions (π-π stacking, salt-bridges, hydrophobic edge) leads to additional electrostatic attractions between the layers, which are then responsible for the compact tetragonal top to bottom layer stacking of the strands. The potential energy surfaces gained after a 10 ns simulation time at pH 7.4 shows that the negative and positive partial charges are optimally oriented in the layered structure, with each layer being predominantly negatively charged on one side and positively charged on the other, thus providing directionality to the stacking of strand layers by electrostatic interactions (Figure S16d). This finding is supported by the observation that the use of the polyanionic contrasting agent PTA for the TEM experiments, which is known for its membrane disrupting tendency,[33] leads to the apparent disintegration of the rods into individual layers (Figures 3b and S12) probably by neutralizing positive layer surface charges. We surmise that the layer stacking is the dominant process of rod assembly formation over the linear growth of the strands, which eventually results in a packing of strands perpendicular to the rod long axis.

Processing and Modelling of pH 3.4 Membrane Structures

We then also used an averaging procedure of a single membrane layer from the cryo-tomographic data in order to reveal the structural features with better signal-to-noise ratio in three dimensions. Figure 4g shows the representation of the corresponding volume stack as a 2D projection image providing a very detailed hexagonal structure pattern. The most interesting result of this reconstruction was that the hexagonal pattern is actually made up of paired (left-handed) super-helical strands (Figure 4d). This becomes directly evident (i) in the particular side-view orientation of the membrane (Figure 4c) or (ii) when the volume reconstruction of Figure 4g is tilted (Figure S15). It can be directly observed that these strands comprise two super-helical strands wrapped around each other (each helix strand having the diameter of a single alpha-helical strand of 1.5 nm as presented in Figure 4f). Figure 4h shows the processed hexagonal volume pattern superimposed with a pair of modelled double super-helices, which fit the pattern in longitudinal direction as well in the side-by-side alignment. The individual super-helical strands have a pitch of 34 nm and a width of 9 nm (thus fitting the thickness of a single membrane layer) and they are phase shifted by 7.15 nm (75.7°) with respect to each other. Double super-helices in the side-by-side arrangement are 17 nm apart but again are phase-shifted by 90°. In this specific spatial arrangement of linear helical assemblies, the generation of the observed hexagonal pattern becomes evident. If projection images of the model data are calculated, the exact density pattern as obtained from the experimental data is reproduced.

MD simulations were initiated with the same starting geometry as discussed for pH 7.4, (Figures 3h,i and S16), except that the glutamic acid residues were fully protonated and only 2 layers with 3 peptide strands each were used (Figure S17). Interestingly, the 10 ns simulation revealed a prominent trend in which the compact packing organization observed for pH 7.4 was dissolved towards the formation of individual strands with an apparent twisted conformation (Figures 4f and S17). Strand elongation was a result of Cy5 contacts, which remained intact throughout the simulation, and hydrogen bonding between the residues in the C-terminal regions of adjacent peptide strands (Figures 4f and S17c).

The prominent H-band of the absorption spectra (Figure 2) suggests that several dye molecules are electronically coupled in the assemblies, in contrast to the strict dimer case observed at pH 7.4. We therefore assume that the lateral packing of strands is stabilized by additional lateral dye interactions. Such an arrangement is realized by the helical repeat of dye pairs (blue dots in Figure 4h), which occupy a repetitive position along the strand axis and allow for an alignment with the dye pairs of the neighboring strands. The suggested assembly of four interacting chromophores appears to be a structural analogue to the tetramer configuration accessed by templating the dyes via a DNA HJ. The spectroscopic characteristics in the present case are very similar. The particular dye interaction would also explain the formation of a two-dimensional structure. Due to the extended two-dimensional geometry of the membranes a uniform orientation in a flow field is not to be expected, so that additional information from LD spectra (Figure S10) about the dye orientation in the assemblies is not readily available.

The offset of helices is puzzling, however, we observe faint densities in the microscopic density maps, which might suggest connections between super-helices like spokes of a ladder. MD simulations indicate at least intermediate cross-links between neighbored twisted strands (Figure S17b). We can only speculate, if in addition to the linear formation of super-helices individual peptides could form such intermediate connections and thus initiate the double super-helix distance. The phase shift of ≈7 nm, however, correlates with the length of an individual peptide molecule.

Conclusion

Within natural light-harvesting systems the surrounding proteins align the chromophores into arrays, which are able of transporting light energy from the antennae to the reaction centers. In recent years considerable effort has been put forth to construct artificial multichromophore systems by applying short DNA-based oligonucleotides as biologically compatible scaffold. Here, we present a molecular construct (**STAP1**) of a Cy5 dye linked to a de novo designed heptad repeat peptide known as one of nature's tools to achieve molecular recognition and efficient self-

assembly, as an alternative to the DNA constructs. The peptide-dye conjugate has the freedom to self-assemble into a supramolecular structure in which not the strict rules of coiled coil formation dictate folding but rather the competing intermolecular forces due to the involved π-systems of dyes in combination with hydrophobic and charged amino acid residues to generate new and fascinating supramolecular structures.

The uniqueness of the particular peptide scaffold was found in its ability (i) to tune the formation of two different H-type aggregates and (ii) to establish a charge pattern of the peptide scaffold so that two completely distinct but exquisitely well-defined ultrastructures can be created on changing the solvent pH from neutral to acidic. Under basic pH conditions J-type aggregates are formed, but these assemblies are only a few nanometers in size, disordered, and, beyond that, non-fluorescent, which makes them less attractive for applications.

AFM and cryogenic electron microscopy revealed that at pH 7.4 rod-like objects with diameters in the 90–300 nm range and lengths up to the micrometer scale are formed. On contrary, flat membrane-like objects with an apparent hexagonal ultrastructure are spontaneously formed at pH 3.4. Based on cryogenic electron microscopic data, MD simulation, and optical spectroscopy we concluded that the electronic coupling between the Cy5 moieties contributes essentially to the formation of the two mesoscopic peptide architectures. The protonation states of lysines and glutamic acids ultimately direct the eventual formation of either rods or two-dimensional membranes.

At neutral pH, the antiparallel linear arrangement of peptide sequences is triggered by chromophore stacking causing the formation of antiparallel double strands by lateral interactions of salt-bridges, whereas hydrophobic leucine edges promote assembly towards two-dimensional layers of the strands. The resulting rotational lock of the double strands, which prevents coiled-coil formation, enables the directional presentation of negative charges of glutamic acid and positive charges of lysines on each side of the strand layer and hence triggers the formation of the observed layer stacks (rods). The arrangement of strands perpendicular to the rod long axis in a tetrameric packing mode is caused by this directed electrostatic stacking process, which obviously dominates over the growth of linear strands. This combination of effects prevents the otherwise expected alignments of strands in a hexagonal packing mode along a rod long axis, as has been reported in several earlier publications.

The protonation of glutamic acid and lysines at pH 3.4, however, eventually interrupts this electrostatically fixed assembly. While maintaining the chromophore stacking the interaction of hydrophobic leucine edges and positively charged lysine residues leads to a drastic change of the overall structure, as it has been supported by MD simulation. There is a trend towards the formation of a superhelical ultrastructure, which enables (i) an additional lateral stacking of the dye chromophores and (ii) a presentation of positive charges towards the surfaces of an extended membrane-like layer. The acidification of the peptide thus creates a kind of polymeric amphiphile (hydrophobic leucine edge vs. hydrophilic (positively charged) lysine residues) which eventually leads to the formation of an assembly structure where the hydrophilic lysine residues are exposed towards the aqueous phase. This effect might explain the observed separation of individual two-dimensional membrane layers due to the charge repulsion of surface exposed lysines.

By using a peptide as template for dye aggregation, we present a novel concept that is an alternative to the established attachment of dyes onto DNA oligomers in mimicking photosynthetic light-harvesting systems. The here described dye-peptide conjugate is capable of forming two novel distinct supramolecular assemblies which are structurally triggered by the complementary interplay of mutual chromophore coupling and pH induced changes in the peptide charge pattern. This dye-peptide system impressively demonstrates how the photo-physical properties of formed aggregate types can be tuned without synthetic modification, solely by changing the environmental conditions. In general, the tuning of dye self-assembly by choosing an appropriate chemistry of a peptide scaffold as well as adapting suitable preparation and environmental conditions opens an avenue for the generation of new biomaterials for further photo-physical research and potential technological applications.

Acknowledgements

We thank the European Union's Seventh Framework Program for research, technological development and demonstration under the Marie Curie ITN Scheme (Fluor21 grant number FP7-PEOPLE-2013-ITN-607787) for financial support. The work of Noureldin Saleh has been financed by the DFG Cluster of Excellence MATH+. We would like to acknowledge the assistance of the Core Facility BioSupraMol supported by the DFG. We thank Drs. Allison A. Berger and Dorian Mikolajczak for proof-reading and for the discussions that improved the manuscript. Open Access funding enabled and organized by Projekt DEAL.

Conflict of Interest

The authors declare no conflict of interest.

Data Availability Statement

The data that support the findings of this study are available in the Supporting Information of this article.

Keywords: Chromophore Assembly · Cyanines · De Novo Peptide · Electron Microscopy · H-Aggregates

[1] a) G. S. Engel, T. R. Calhoun, E. L. Read, T. K. Ahn, T. Mančal, Y. C. Cheng, R. E. Blankenship, G. R. Fleming,

Nature **2007**, *446*, 782–786; b) G. D. Scholes, G. R. Fleming, A. Olaya-Castro, R. Van Grondelle, *Nat. Chem.* **2011**, *3*, 763–774; c) H. W. Rathbone, J. A. Davis, K. A. Michie, S. C. Goodchild, N. O. Robertson, P. M. G. Curmi, *Biophys. Rev. Lett.* **2018**, *10*, 1427–1441.

[2] a) O. Ostroverkhova, *Chem. Rev.* **2016**, *116*, 13279–13412; b) T. Brixner, R. Hildner, J. Köhler, C. Lambert, F. Würthner, *Adv. Energy Mater.* **2017**, *7*, 1700236.

[3] B. L. Cannon, D. L. Kellis, P. H. Davis, J. Lee, W. Kuang, W. L. Hughes, E. Graugnard, B. Yurke, W. B. Knowlton, *ACS Photonics* **2015**, *2*, 398–404.

[4] a) H.-W. An, L.-L. Li, Y. Wang, Z. Wang, D. Hou, Y.-X. Lin, S.-L. Qiao, M.-D. Wang, C. Yang, Y. Cong, Y. Ma, X.-X. Zhao, Q. Cai, W.-T. Chen, C.-Q. Lu, W. Xu, H. Wang, Y. Zhao, *Nat. Commun.* **2019**, *10*, 4861; b) Y. Li, Y. Zhou, X. Yue, Z. Dai, *Adv. Healthcare Mater.* **2020**, *9*, 2001327; c) R. S. Gamage, D.-H. Li, C. L. Schreiber, B. D. Smith, *ACS Omega* **2021**, *6*, 30130–30139; d) Y. Deng, W. Zhan, G. Liang, *Adv. Healthcare Mater.* **2021**, *10*, 200121.

[5] a) Y. N. Teo, E. T. Kool, *Chem. Rev.* **2012**, *112*, 4221–4245; b) É. Boulais, N. P. D. Sawaya, R. Veneziano, A. Andreoni, J. L. Banal, T. Kondo, S. Mandal, S. Lin, G. S. Schlau-Cohen, N. W. Woodbury, H. Yan, A. Aspuru-Guzik, M. Bathe, *Nat. Mater.* **2018**, *17*, 159–166; c) X. Zhou, S. Mandal, S. Jiang, S. Lin, J. Yang, Y. Liu, D. G. Whitten, N. W. Woodbury, H. Yan, *J. Am. Chem. Soc.* **2019**, *141*, 8473–8481; d) T. Schröder, M. B. Scheible, F. Steiner, J. Vogelsang, P. Tinnefeld, *Nano Lett.* **2019**, *19*, 1275–1281; e) O. A. Mass, C. K. Wilson, S. K. Roy, M. S. Barclay, L. K. Patten, E. A. Terpetschnig, J. Lee, R. D. Pensack, B. Yurke, W. B. Knowlton, *J. Phys. Chem. B* **2020**, *124*, 9636–9647; f) S. M. Hart, W. J. Chen, J. L. Banal, W. P. Bricker, A. Dodin, L. Markova, Y. Vyborna, A. P. Willard, R. Häner, M. Bathe, G. S. Schlau-Cohen, *Chem* **2021**, *7*, 752–773; g) M. S. Barclay, S. K. Roy, J. S. Huff, O. A. Mass, D. B. Turner, C. K. Wilson, D. L. Kellis, E. A. Terpetschnig, J. Lee, P. H. Davis, B. Yurke, W. B. Knowlton, R. D. Pensack, *Commun. Chem.* **2021**, *4*, 19; h) J. Gorman, S. R. E. Orsborne, A. Sridhar, R. Pandya, P. Budden, A. Ohmann, N. A. Panjwani, Y. Liu, J. L. Greenfield, S. Dowland, V. Gray, S. T. J. Ryan, S. De Ornellas, A. H. El-Sagheer, T. Brown, J. R. Nitschke, J. Behrends, U. F. Keyser, A. Rao, R. Collepardo-Guevara, E. Stulz, R. H. Friend, F. Auras, *J. Am. Chem. Soc.* **2022**, *144*, 368–376; i) J. Dietzsch, D. Bialas, J. Bandorf, F. Würthner, C. Höbartner, *Angew. Chem. Int. Ed.* **2022**, *61*, e202116783; *Angew. Chem.* **2022**, *134*, e202116783.

[6] a) M. Wang, G. L. Silva, B. A. Armitage, *J. Am. Chem. Soc.* **2000**, *122*, 9977–9986; b) A. Iqbal, S. Arslan, B. Okumus, T. J. Wilson, G. Giraud, D. G. Norman, T. Ha, D. M. J. Lilley, *Proc. Natl. Acad. Sci. USA* **2008**, *105*, 11176–11181; c) F. Nicoli, M. K. Roos, E. A. Hemmig, M. Di Antonio, R. de Vivie-Riedle, T. Liedl, *J. Phys. Chem. A* **2016**, *120*, 9941–9947; d) J. L. Banal, T. Kondo, R. Veneziano, M. Bathe, G. S. Schlau-Cohen, *J. Phys. Chem. Lett.* **2017**, *8*, 5827–5833; e) B. L. Cannon, L. K. Patten, D. L. Kellis, P. H. Davis, J. Lee, E. Graugnard, B. Yurke, W. B. Knowlton, *J. Phys. Chem. A* **2018**, *122*, 2086–2095; f) P. D. Cunningham, S. A. Díaz, B. Yurke, I. L. Medintz, J. S. Melinger, *J. Phys. Chem. B* **2020**, *124*, 8042–8049; g) R. J. Mazuski, S. A. Díaz, R. E. Wood, L. T. Lloyd, W. P. Klein, D. Mathur, J. S. Melinger, G. S. Engel, I. L. Medintz, *J. Phys. Chem. Lett.* **2020**, *11*, 4163–4172; h) D. Mathur, A. Samanta, M. G. Ancona, S. A. Díaz, Y. Kim, J. S. Melinger, E. R. Goldman, J. P. Sadowski, L. L. Ong, P. Yin, I. L. Medintz, *ACS Nano* **2021**, *15*, 16452–16468; i) D. Heussman, J. Kittell, P. H. von Hippel, A. H. Marcus, *J. Chem. Phys.* **2022**, *156*, 045101.

[7] M. Kube, F. Kohler, E. Feigl, B. Nagel-Yüksel, E. M. Willner, J. J. Funke, T. Gerling, P. Stömmer, M. N. Honemann, T. G. Martin, S. H. W. Scheres, H. Dietz, *Nat. Commun.* **2020**, *11*, 6229.

[8] a) W. Kühlbrandt, *Science* **2014**, *343*, 1443–1444; b) T. Nakane, A. Kotecha, A. Sente, G. McMullan, S. Masiulis, P. M. G. E. Brown, I. T. Grigoras, L. Malinauskaite, T. Malinauskas, J. Miehling, T. Uchański, L. Yu, D. Karia, E. V. Pechnikova, E. de Jong, J. Keizer, M. Bischoff, J. McCormack, P. Tiemeijer, S. W. Hardwick, D. Y. Chirgadze, G. Murshudov, A. R. Aricescu, S. H. W. Scheres, *Nature* **2020**, *587*, 152–156; c) K. M. Yip, N. Fischer, E. Paknia, A. Chari, H. Stark, *Nature* **2020**, *587*, 157–161; d) T. H. Sharp, M. Bruning, J. Mantell, R. B. Sessions, A. R. Thomson, N. R. Zaccai, R. L. Brady, P. Verkade, D. N. Woolfson, *Proc. Natl. Acad. Sci. USA* **2012**, *109*, 13266–13271; e) L. Pieri, F. Wang, A.-A. Arteni, M. Vos, J.-M. Winter, M.-H. Le Du, F. Artzner, F. Gobeaux, P. Legrand, Y. Boulard, S. Bressanelli, E. H. Egelman, M. Paternostre, *Proc. Natl. Acad. Sci. USA* **2022**, *119*, e2120346119; f) S. H. Yoo, H.-S. Lee, *Acc. Chem. Res.* **2017**, *50*, 832–841.

[9] a) K. J. Channon, G. L. Devlin, C. E. MacPhee, *J. Am. Chem. Soc.* **2009**, *131*, 12520–12521; b) R. Zheng, J. Yang, M. Mamuti, D.-Y. Hou, H.-W. An, Y. Zhao, H. Wang, *Angew. Chem. Int. Ed.* **2021**, *60*, 7809–7819; *Angew. Chem.* **2021**, *133*, 7888–7898; c) B. Liu, Y. Vonhausen, A. Schulz, C. Höbartner, F. Würthner, *Angew. Chem. Int. Ed.* **2022**, *61*, e202200120; *Angew. Chem.* **2022**, *134*, e202200120.

[10] a) A. Pena-Francesch, M. C. Demirel, *Front. Chem.* **2019**, *7*, 69; b) E. H. C. Bromley, K. Channon, E. Moutevelis, D. N. Woolfson, *ACS Chem. Biol.* **2008**, *3*, 38–50.

[11] a) R. B. Merrifield, *J. Am. Chem. Soc.* **1963**, *85*, 2149–2154; b) J. M. Humphrey, A. R. Chamberlin, *Chem. Rev.* **1997**, *97*, 2243–2266.

[12] a) M. Mutter, R. Gassmann, U. Buttkus, K.-H. Altmann, *Angew. Chem. Int. Ed. Engl.* **1991**, *30*, 1514–1516; *Angew. Chem.* **1991**, *103*, 1504–1506; b) S. Zhang, A. Rich, *Proc. Natl. Acad. Sci. USA* **1997**, *94*, 23–28; c) J. D. Hartgerink, E. Beniash, S. I. Stupp, *Science* **2001**, *294*, 1684–1688; d) J. H. Collier, B.-H. Hu, J. W. Ruberti, J. Zhang, P. Shum, D. H. Thompson, P. B. Messersmith, *J. Am. Chem. Soc.* **2001**, *123*, 9463–9464; e) D. J. Pochan, J. P. Schneider, J. Kretsinger, B. Ozbas, K. Rajagopal, L. Haines, *J. Am. Chem. Soc.* **2003**, *125*, 11802–11803.

[13] a) R. J. Mart, R. D. Osborne, M. M. Stevens, R. V. Ulijn, *Soft Matter* **2006**, *2*, 822–835; b) D. W. P. M. Löwik, E. H. P. Leunissen, M. Van Den Heuvel, M. B. Hansen, J. C. M. Van Hest, *Chem. Soc. Rev.* **2010**, *39*, 3394–3412; c) K. Pagel, B. Koksch, *Curr. Opin. Chem. Biol.* **2008**, *12*, 730–739.

[14] a) M. Zhou, D. Bentley, I. Ghosh, *J. Am. Chem. Soc.* **2004**, *126*, 734–735; b) D. Papapostolou, A. M. Smith, E. D. T. Atkins, S. J. Oliver, M. G. Ryadnov, L. C. Serpell, D. N. Woolfson, *Proc. Natl. Acad. Sci. USA* **2007**, *104*, 10853–10858.

[15] I. W. Hamley, *Angew. Chem. Int. Ed.* **2014**, *53*, 6866–6881; *Angew. Chem.* **2014**, *126*, 6984–7000.

[16] W. A. Petka, J. L. Harden, K. P. McGrath, D. Wirtz, D. A. Tirrell, *Science* **1998**, *281*, 389–392.

[17] F. Würthner, T. E. Kaiser, C. R. Saha-Möller, *Angew. Chem. Int. Ed.* **2011**, *50*, 3376–3410; *Angew. Chem.* **2011**, *123*, 3436–3473.

[18] "The morphologies of molecular cyanine dye aggregates as revealed by cryogenic transmission electron microscopy": H. von Berlepsch, C. Böttcher in *J-aggregates, Vol. 2* (Ed.: T. Kobayashi), World Scientific, Singapore, **2012**, p. 119.

[19] a) M. Levitus, S. Ranjit, *Q. Rev. Biophys.* **2011**, *44*, 123–151; b) U. Lewandowska, W. Zajaczkowski, S. Corra, J. Tanabe, R. Borrmann, E. M. Benetti, S. Stappert, K. Watanabe, N. A. K. Ochs, R. Schaeublin, C. Li, E. Yashima, W. Pisula, K. Müllen, H. Wennemers, *Nat. Chem.* **2017**, *9*, 1068–1072.

[20] a) E. Zacco, C. Anish, C. E. Martin, H. von Berlepsch, E. Brandenburg, P. H. Seeberger, B. Koksch, *Biomacromolecules* **2015**, *16*, 2188–2197; b) E. Zacco, J. Hütter, J. L. Heier, J. Mortier, P. H. Seeberger, B. Lepenies, B. Koksch, *ACS Chem. Biol.* **2015**, *10*, 2065–2072.
[21] P. B. Harbury, T. Zhang, P. S. Kim, T. Alber, *Science* **1993**, *262*, 1401–1407.
[22] J. M. Mason, K. M. Arndt, *ChemBioChem* **2004**, *5*, 170–176.
[23] "The design of coiled-coil structures and assemblies": D. N. Woolfson, *Advances in Protein Chemistry*, Academic Press, New York, **2005**, pp. 79–112.
[24] A. Fegan, P. S. Shirude, S. Balasubramanian, *Chem. Commun.* **2008**, 2004–2006.
[25] H. von Berlepsch, C. Böttcher, *J. Phys. Chem. B* **2015**, *119*, 11900–11909.
[26] H. von Berlepsch, C. Böttcher, *Phys. Chem. Chem. Phys.* **2018**, *20*, 18969–18977.
[27] C. Gribbon, K. J. Channon, W. Zhang, E. F. Banwell, E. H. C. Bromley, J. B. Chaudhuri, R. O. C. Oreffo, D. N. Woolfson, *Biochemistry* **2008**, *47*, 10365–10371.
[28] a) C. Bustamante, I. Tinoco, Jr., M. F. Maestre, *Proc. Natl. Acad. Sci. USA* **1983**, *80*, 3568–3572; b) M. J. Pandya, G. M. Spooner, M. Sunde, J. R. Thorpe, A. Rodger, D. N. Woolfson, *Biochemistry* **2000**, *39*, 8728–8734.
[29] J. Kang, O. Kaczmarek, J. Liebscher, L. Dähne, *Int. J. Polym. Sci.* **2010**, *1*, 264781.
[30] a) M. Nambiar, L.-S. Wang, V. Rotello, J. Chmielewski, *J. Am. Chem. Soc.* **2018**, *140*, 13028–13033; b) A. M. Smith, E. F. Banwell, W. R. Edwards, M. J. Pandya, D. N. Woolfson, *Adv. Funct. Mater.* **2006**, *16*, 1022–1030; c) H. V. Zhang, F. Polzer, M. J. Haider, Y. Tian, J. A. Villegas, K. L. Kiick, D. J. Pochan, J. G. Saven, *Sci. Adv.* **2016**, *2*, e1600307.
[31] I. Amenabar, S. Poly, W. Nuansing, E. H. Hubrich, A. A. Govyadinov, F. Huth, R. Krutokhvostov, L. Zhang, M. Knez, J. Heberle, A. M. Bittner, R. Hillenbrand, *Nat. Commun.* **2013**, *4*, 2890.
[32] R. L. Thurlkill, G. R. Grimsley, J. M. Scholtz, C. N. Pace, *Protein Sci.* **2006**, *15*, 1214–1218.
[33] W. P. Cunningham, L. A. Staehelin, R. W. Rubin, R. Wilkins, M. Bonneville, *J. Cell Biol.* **1974**, *62*, 491–504.

Manuscript received: June 13, 2022
Accepted manuscript online: September 26, 2022
Version of record online: October 26, 2022